

Independent indistinguishable quantum light sources on a reconfigurable photonic integrated circuit

D. J. P. Ellis, A. J. Bennett, C. Dangel, J. P. Lee, J. P. Griffiths, T. A. Mitchell, T.-K. Paraiso, P. Spencer, D. A. Ritchie, and A. J. Shields

Citation: *Appl. Phys. Lett.* **112**, 211104 (2018); doi: 10.1063/1.5028339

View online: <https://doi.org/10.1063/1.5028339>

View Table of Contents: <http://aip.scitation.org/toc/apl/112/21>

Published by the American Institute of Physics

Articles you may be interested in

Radio-over-fiber using an optical antenna based on Rydberg states of atoms

Applied Physics Letters **112**, 211106 (2018); 10.1063/1.5031033

Graphene quantum blisters: A tunable system to confine charge carriers

Applied Physics Letters **112**, 213101 (2018); 10.1063/1.5023896

Simple method for the characterization of intense Laguerre-Gauss vector vortex beams

Applied Physics Letters **112**, 211103 (2018); 10.1063/1.5027661

Airborne ultrasound surface motion camera: Application to seismocardiography

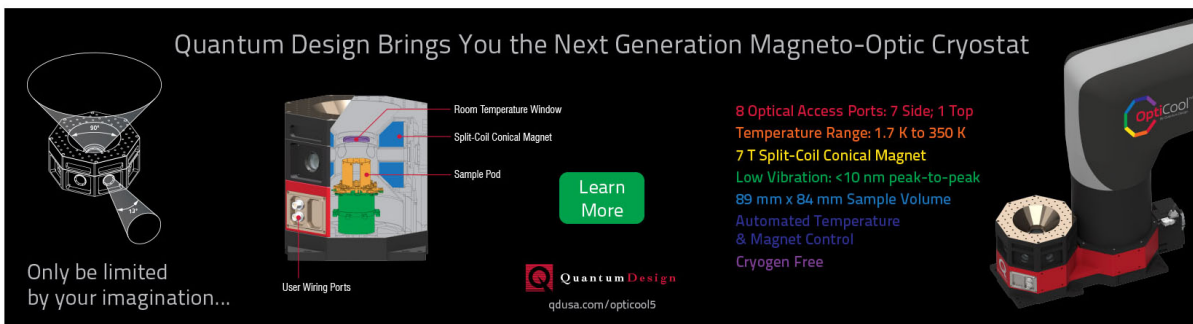
Applied Physics Letters **112**, 213702 (2018); 10.1063/1.5028348

Electrically driven and electrically tunable quantum light sources

Applied Physics Letters **110**, 071102 (2017); 10.1063/1.4976197

Thin-film nano-thermogravimetry applied to praseodymium-cerium oxide films at high temperatures

Applied Physics Letters **112**, 213502 (2018); 10.1063/1.5025389



Quantum Design Brings You the Next Generation Magneto-Optic Cryostat

Only be limited by your imagination...

Room Temperature Window
Split-Coil Conical Magnet
Sample Pod
User Wiring Ports

Learn More

8 Optical Access Ports: 7 Side; 1 Top
Temperature Range: 1.7 K to 350 K
7 T Split-Coil Conical Magnet
Low Vibration: <10 nm peak-to-peak
89 mm x 84 mm Sample Volume
Automated Temperature & Magnet Control
Cryogen Free

Quantum Design
qdusa.com/opticool5

The advertisement features a large image of the Quantum Design OptiCool cryostat, which is a black cylindrical device with a red base and a circular top access port. To the left, there's a smaller diagram of the cryostat with various ports labeled: Room Temperature Window, Split-Coil Conical Magnet, Sample Pod, and User Wiring Ports. Below this diagram is a green button labeled "Learn More". At the bottom left, there's a quote: "Only be limited by your imagination...". On the right side, there's a detailed technical specification list. The Quantum Design logo and website address are at the bottom.

Independent indistinguishable quantum light sources on a reconfigurable photonic integrated circuit

D. J. P. Ellis,^{1,a)} A. J. Bennett,^{1,b)} C. Dangel,^{1,c)} J. P. Lee,^{1,d)} J. P. Griffiths,¹ T. A. Mitchell,² T.-K. Paraiso,¹ P. Spencer,² D. A. Ritchie,² and A. J. Shields¹

¹Toshiba Research Europe Limited, 208 Science Park, Milton Road, Cambridge CB4 0GZ, United Kingdom

²Cavendish Laboratory, Cambridge University, J. J. Thomson Avenue, Cambridge CB3 0HE, United Kingdom

(Received 9 March 2018; accepted 24 April 2018; published online 22 May 2018)

We report a compact, scalable, quantum photonic integrated circuit realised by combining multiple, tuneable InGaAs/GaAs quantum dot single photon sources with a silicon oxynitride waveguide circuit. Each waveguide in the circuit is addressed by a separate, electrically controlled quantum dot-containing diode. We show that the quantum dot emission from neighbouring diodes can be independently tuned to degeneracy using the Stark Effect and that the resulting photon streams are indistinguishable. This enables on-chip Hong-Ou-Mandel-type interference, as required for many photonic quantum information processing schemes. © 2018 Author(s). All article content, except where otherwise noted, is licensed under a Creative Commons Attribution (CC BY) license (<http://creativecommons.org/licenses/by/4.0/>). <https://doi.org/10.1063/1.5028339>

Photonic Integrated Circuits (PICs) are rapidly becoming the default platform for photonic quantum applications due to their robustness, interferometric stability, reconfigurability, and scalability.^{1–3} Furthermore, they allow complex optical systems which, until recently, would occupy a whole laboratory to be reduced to the size of a single chip.

PICs have been employed in many quantum applications including logic gates,^{2,4} higher order path entanglement,⁵ quantum walks,^{6,7} tests of Boson Sampling,^{8–11} and on-chip quantum teleportation.¹² These PICs can support optical qubits encoded in path, time bin, polarisation or mode and can be interconverted.^{13,14} All of these experiments have relied upon photons generated externally and delivered to the PICs through fibre.

One route to achieve on-chip photon generation is to use silicon waveguides to directly produce photons,^{15,16} but the Poissonian statistics of pair generation makes this inherently unscalable. An alternative scheme is to use quantum emitters with naturally sub-Poissonian photon statistics within a waveguide circuit made of the emitter's host material.^{17–20} It is also possible to evanescently couple the emitter to a low-loss PIC^{21–23} and these schemes have verified the emission of single photons. However, for realising large scale and compact circuits, it will be necessary to integrate multiple sources of indistinguishable photons on the chip, as we demonstrate here.

The device we report utilises a “plug, bond and play” approach to passively align and join multiple, independent quantum light sources to a PIC in an inherently scalable fashion. The Quantum Photonic Integrated Circuit, or QPIC, consists of three parts as shown in Fig. 1: (1) an array of Quantum

Dot (QD)-containing diodes, which are butt-coupled to (2) a reconfigurable silicon oxynitride (SiO_xN_y) PIC on a silicon substrate and (3) an array of optical fibres. We show the essential elements of a QPIC including the generation of coherent, indistinguishable quantum light on-chip; reconfigurability; and the inclusion of an integrated excitation source.

The linear array of independently controllable QD diodes can naturally emit single photons, photon pairs^{24,25} and using electric field tuning, transitions in separate emitters can be made degenerate. The diodes are rotated through 90° in order to butt-couple to the PIC. We achieve electrical connection to the diodes using gold tracks on the surface of the PIC, and a series of metal filled recesses at the left-hand end of the PIC. Raised metal contacts on the diodes mate with these etched recesses to form a “plug and socket”

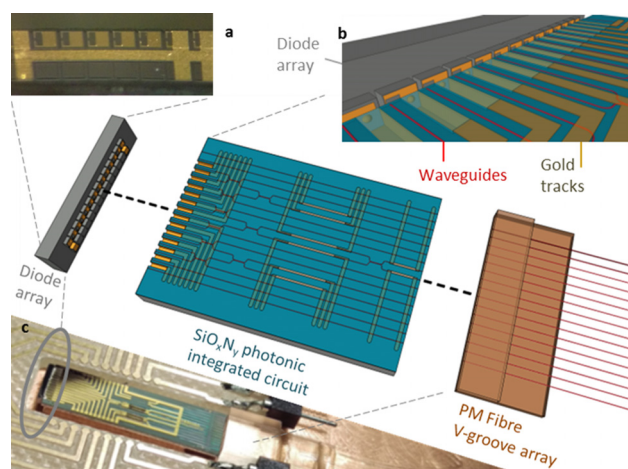


FIG. 1. Assembly of the Quantum Photonic Integrated Circuit. The main figure shows an exploded diagram of the diode array, the SiO_xN_y waveguide circuit, and the PM fibre array. (a) Optical photograph showing part of the diode array. The five central mesas in the top row are optically active devices. The outer three (linked) pairs are dummy mesas used to electrically connect the lower doped layer of the diode. Mesas are on a 250 μm pitch. (b) Schematic of the bonding interface between the diode array and waveguide circuit. (c) Optical photograph of the assembled device. For scale, dimensions of the waveguide chip are 17 \times 8 mm.

^{a)}Author to whom correspondence should be addressed: david.ellis@crl.toshiba.co.uk

^{b)}Now at School of Engineering, Cardiff University, Queen's Buildings, 14-17 The Parade, Cardiff CF24 3AA, United Kingdom.

^{c)}Also at Physik Department, Technische Universität München, 85748 Garching, Germany.

^{d)}Also at Department of Engineering, Cambridge University, 9 J.J. Thomson Avenue, Cambridge CB3 0FA, United Kingdom.

arrangement, aligning the diodes and waveguides. The whole device can then be mounted on a “dip stick” and lowered directly into helium vapour, cooling the device to 8 K. Under these conditions, all ten of the diodes and the phase modulators can be operated simultaneously.

The diode heterostructure, grown by molecular beam epitaxy, comprises a weak planar cavity with 4 (10) pairs of GaAs/AlGaAs distributed Bragg reflectors above (below) a λ -cavity spacer. Self-assembled InAs quantum dots are placed at the centre of the cavity with an AlGaAs tunnel barrier on both sides. This “dot-in-a-well” configuration allows the quantum dot emission wavelength to be electrically tuned over 10 s of nms under reverse bias.²⁴ Under forward bias, electroluminescence from the QDs and wetting layer will be emitted. The upper p-contact is partially covered with a gold contact, upon which a $\sim 70 \mu\text{m}$ diameter gold ball bump is placed. This bump forms the male part of the “plug and socket” assembly scheme. Additional mesas are used to access the lower ohmic contact. These can be seen at each end of the array shown in Fig. 1(a).

The photonic integrated circuit comprises a $1.6 \mu\text{m}$ thick core layer of $n = 1.55$ SiO_xN_y , surrounded by $n = 1.51$ SiO_xN_y supporting a single mode at 900 nm. All of the SiO_xN_y

layers are deposited by Plasma Enhanced Chemical Vapour Deposition (PECVD) onto a silicon substrate. Waveguides are defined lithographically and dry etched prior to the deposition of the overcladding layer. Further etching of the SiO_xN_y and underlying silicon is then used to form thermal isolation trenches for the phase modulators and the “sockets” for the interconnection of the diodes. Finally, metal layers are deposited and patterned by lift-off to form the various contact tracks and resistive heaters for the Mach-Zehnder interferometers (MZIs).

The fibre array comprises an array of 20 polarisation-maintaining optical fibres. The fibres are used both to route in laser light, when off-chip optical excitation is employed, and to collect QD emission.

The fibre- and diode-arrays are bonded to the PIC using an index-matched UV-curable adhesive. The raised contours of the plug-and-socket configuration also prevent the bonding adhesive from encapsulating the contact areas. The trench is then filled with a silver-doped conductive epoxy to complete the electrical link from the surface of the PIC to each diode. This hybrid assembly scheme can be consistently reproduced with 100% yield of the 20 electrical interconnects. The waveguides, diodes, and fibres are all arranged on a $250 \mu\text{m}$ pitch.

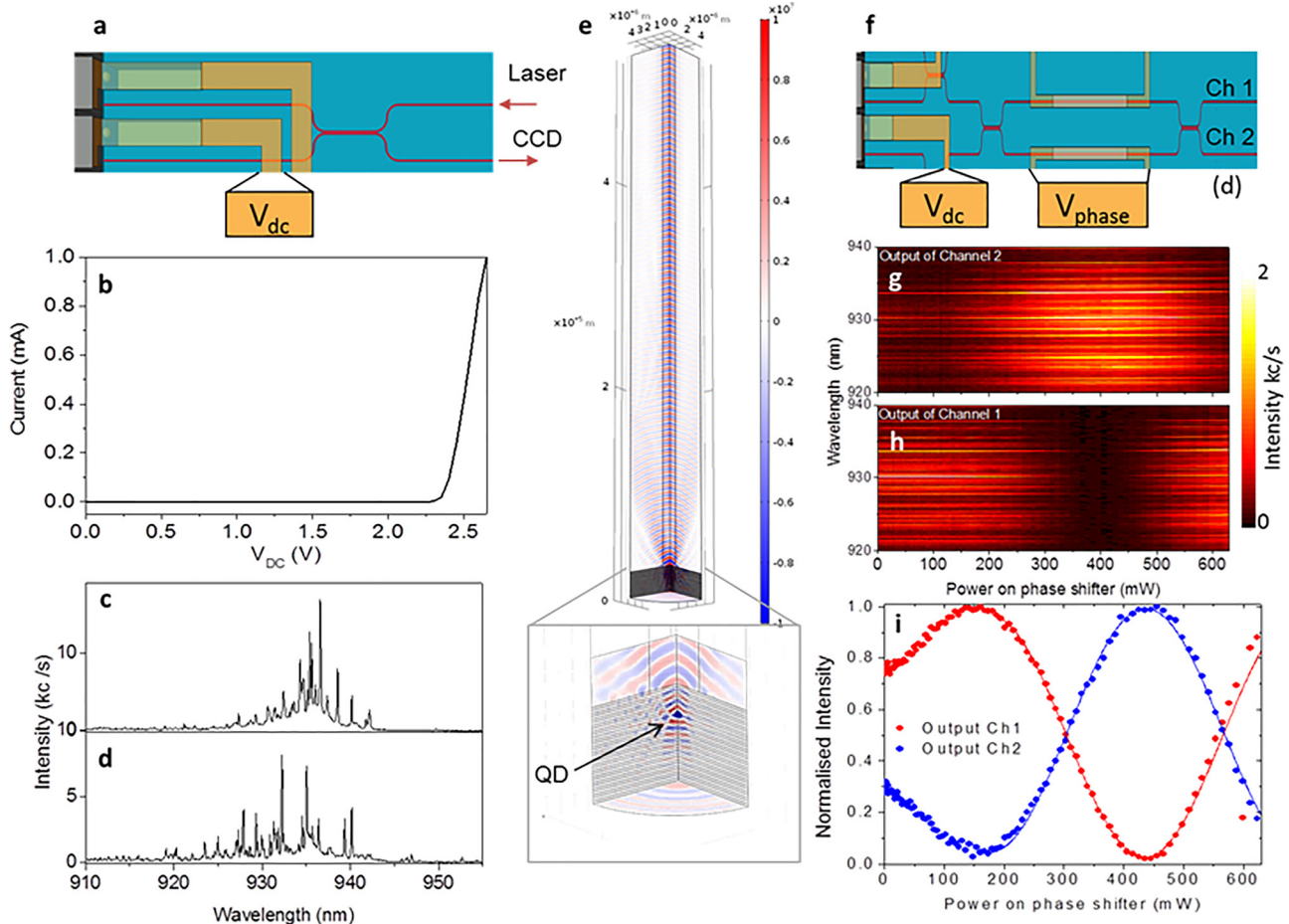


FIG. 2. Activating and redirecting light on the Quantum Photonic Integrated Circuit. (a) Schematic of the operation of the device under external optical excitation. (b) Typical IV curve. (c) and (d) Photoluminescence spectra recorded from two diodes at 1.0V. (e) Finite Element Method simulation showing coupling between an on-axis quantum dot in a low-quality planar cavity and a butt-coupled straight waveguide. The lower part of the figure shows a magnified view of the semiconductor cavity, quantum dot, and the initial launch into the waveguide. For the device used in this work, we expect a coupling efficiency of 8%. (f) Schematic showing operation of the on-chip phase shifters. (g) and (h) Electroluminescence from one diode measured through channels 1 and 2, respectively, as the power applied to the phase shifter is varied. A clear switching behaviour is observed. (i) Single wavelength (890 nm) data from (e) replotted in more detail. We observe \sim ideal MZI behaviour.

One section of the QPIC is as shown in Fig. 2(a), with two diodes addressing a directional coupler. Figure 2(b) shows a typical IV curve. Photo-luminescence from each diode in the pair can be separately measured by biasing the unwanted device at -5 V to quench its emission [Figs. 2(c) and 2(d)]. In Fig. 2(a), an external 850 nm excitation laser is routed in through the waveguide circuit to pump both diodes. Only emission from QDs aligned with the waveguide can contribute to the collected spectra. We employ a relatively high density of QDs ($\sim 3/\mu\text{m}^2$) to ensure that several QDs couple to each waveguide. Figure 2(e) shows a Finite Element Method calculation of the electric field, E , from an on-axis QD coupled into a waveguide. The efficiency of light collection from the device is influenced by the numerical aperture of the waveguide ($\text{NA} = 0.35$ here), giving a similar efficiency to what would be expected from a free-space lens of the same numerical aperture.²⁶ Simulations indicate the coupling efficiency between an on-axis QD and the waveguide is 8%.

The collection area can be changed by modifying the width of the waveguide at the PIC/diode interface. Increasing the width will allow light from more off-axis QDs to be coupled into the waveguide at the expense of absolute

collection efficiency. Reducing the width of the waveguide increases the collection efficiency to $\sim 40\%$, limited by the refractive index contrast between GaAs and the waveguide core. However, achieving these efficiencies would require site controlled QDs precisely aligned on-axis with each waveguide channel.^{27,28}

Networks of phase shifters and MZIs may be used to realise any arbitrary circuit³ and prepare arbitrary rail-encoded qubits. This QPIC features a reconfigurable MZI, with a lithographically defined resistive heater [Fig. 2(f)]. In Figs. 2(g) and 2(h), we drive one device in forward bias to emit electroluminescence to calibrate the MZI. Scanning the power applied to the phase shifter produces a clear switching between the output ports. At 890 nm, we observe ideal switching operation [Fig. 2(i)] with a visibility greater than 98%. Such high fidelity single qubit manipulation is an essential element of any reconfigurable QPIC. A 2π phase shift requires a 520 mW electrical input to the phase modulator. This is limited by the thermal conductivity of the $5\ \mu\text{m}$ overcladding layer. Placing the heater element closer to the waveguide core would reduce the power requirements by a factor of 10.

The diodes are designed to allow a giant Stark shift of >20 nm (Ref. 24) in reverse bias. In this regime, no current

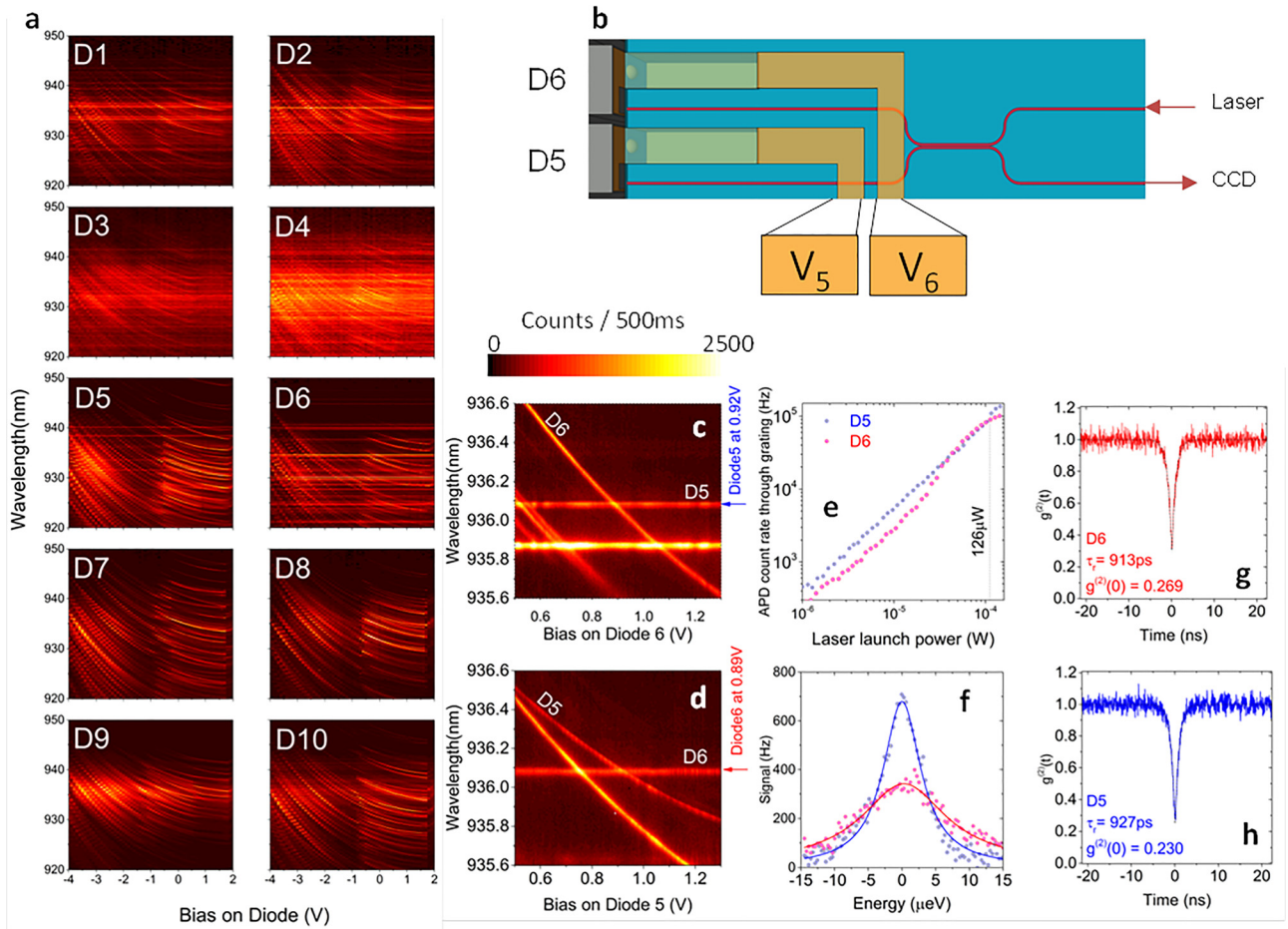


FIG. 3. Making the transitions in separated emitters degenerate. (a) Photoluminescence vs bias scans of all 10 diodes on the device. All show similar tuning behaviour. The intensity of the recorded spectra is normalised. (b) Schematic of the device with diodes D5 and D6, which is studied in more detail. (c) PL tuning curve. D5 held at 0.92 V. Bias applied to D6 is scanned. (d) PL tuning curve. As for (c) except D5 is now scanned and D6 is held constant. (e) Photoluminescence power dependence for the transitions at degeneracy. With a launch pump power of $126\ \mu\text{W}$, both emission lines have the same intensity. This excitation power is used for all subsequent measurements. (f) Etalon linewidth measurements at degeneracy. The solid lines are Lorentzian fits to the data. (g) and (h) Autocorrelation histograms for diodes D5 and D6, respectively.

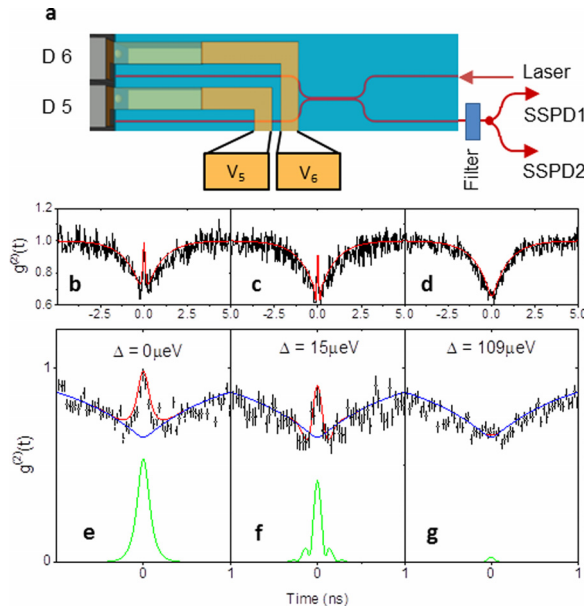


FIG. 4. On-chip two photon interference of light from separate diodes. (a) The experimental setup for testing the indistinguishability of light from diodes D5 and D6. (b)–(d) Experimental Hong-Ou-Mandel histograms for detunings of 0, 15, and 109 μeV between the two quantum dot transitions, which are enlarged in (e)–(g). The red (blue) line is a calculation based on experimental parameters when maximum (minimum) indistinguishability is present. These agree well with the experimental data. The green line plots the predicted visibility.

flows and no electroluminescence is observed. Under optical excitation, all diodes on the QPIC exhibit similar behaviour, as shown in Fig. 3(a). We observe transitions from predominantly neutral and positively charged states below -1 V and predominantly negatively charged states above.²⁹

We select two adjacent diodes, D5 and D6, to demonstrate that photons from separated QDs can be rendered indistinguishable. Both were simultaneously optically excited through the waveguide circuit and QD photons collected through a single channel, as shown in Fig. 3(b). Figure 3(c) shows tuning of D6 with a bias on D5 = 0.92 V and in Fig. 3(d), the bias on D5 is varied whilst D6 = 0.89 V. We are able to tune negatively charged transitions to degeneracy at 936.1 nm when $V_{D5} = 0.92\text{ V}$ and $V_{D6} = 0.89\text{ V}$. We then separately characterise the transitions, suppressing emission from the other device by applying -5 V . The transitions display a different power dependence, having the same intensity of

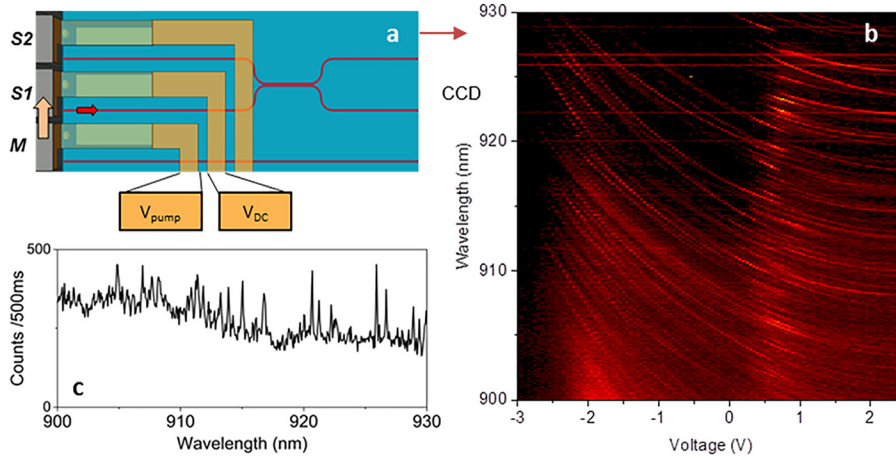


FIG. 5. Integrating the excitation source onto the QPIC. (a) Schematic of the section of the device used to demonstrate simultaneous on-chip pumping and tuning of a quantum emitter. A bias of V_{pump} is applied to the Master LED (M), and strong emission at 880 nm is guided to two adjacent Slave diodes ($S1, S2$). One of these is tuned by bias V_{DC} to produce the plot in (b) and (c) is a cut through b at a bias of 0 V.

10^5 Hz with $126\text{ }\mu\text{W}$ pump laser power (measured through a transmission grating with 50% transmission efficiency on a Silicon APD). The QD transitions were not at saturation. The linewidths of the transitions were then measured using an etalon and coherence times were determined to be 220 ps and 100 ps, respectively [Fig. 3(f)]. While spectral jitter and other mechanisms can result in inhomogeneous broadening of the measured peak, the high quality of the Lorentzian fits indicates that the measured linewidth is dominated by homogeneous broadening. Using a Hanbury Brown and Twiss setup and a pair of superconducting single photon detectors, the measured anti-bunching times of the two transitions in D5 (D6) were 913 ps (927 ps) and $g^{(2)}(0)$ was 0.230 (0.269) [Figs. 3(g) and 3(h)]. Non-zero $g^{(2)}(0)$ may be attributed to background emission from other QDs in each device.

We then perform a Hong-Ou-Mandel experiment to study on-chip two photon interference. With both devices tuned to degeneracy, if indistinguishable, photons from the two QDs will undergo two-photon interference at the directional coupler and both leave from the same output port of the QPIC. If both photons do leave from the same output port of the directional coupler, we should see an increased probability of coincidences with zero time delay, manifested as a peak at $t = 0$ overlaid on top of the autocorrelation histogram observed when no interference takes place. Figure 4(b) show the experimental data recorded under these conditions. The peak at $t = 0$ is clearly visible.

Using the independently measured characteristics for the two transitions [$[g^{(2)}(0), \text{ radiative lifetime, and coherence time}]$, we calculate the expected autocorrelation,²⁴ shown as red lines in Fig. 4. The model agrees well with the experimental data. For comparison, the blue curve shows the results when no interference takes place. When we introduced a small energy difference between the transitions, the visibility of interference falls [green curve in Figs. 4(e)–4(g)]. At zero detuning, and with infinitely fast detectors, we predict a maximum two photon interference visibility of 80% limited by the non-zero $g^{(2)}(0)$ of the sources. Taking into account the measured detector response, the model predicts a reduced visibility of 54%, in agreement with the experiment.

Finally, Fig. 5 shows how the diode array itself can also be used to simultaneously excite and tune the energy of dots, without an external laser.³⁰ The lower (Master, M) device Fig. 5(a) is driven at 10 mA generating predominantly

~880 nm wetting layer emission that was guided laterally by the cavity. This excites QDs in the adjacent devices (Slave diodes S1, S2), which can be tuned. In Fig. 5(b), light collected from the upper diode (S2, held at fixed bias) occurs at a constant wavelength, but light from the lower diode (S1, biased with V_{DC}) displays the giant stark shift. The diode array used here was not designed with this sort of on-chip excitation in mind, and is not efficient enough to saturate the QD emission lines. A fraction of the pump light is scattered into the waveguides, resulting in the observed background. Reducing the spacing between mesas and modifying the design of the metallic surface layers will improve the pumping efficiency and eliminate stray light in the waveguide channels. This all electrical, tunable excitation scheme therefore offers a route to a truly independent and scalable all electrical QPIC.

Future implementations of the current prototypes on low QD density wafers will eliminate the finite background in $g^{(2)}(\tau)$ measurements. A 10 dB reduction of the background would lead to a 2-photon interference visibility of 98%. Further optimisation of the waveguide profile at the diode/PIC interface, deterministic QD positioning^{27,28} and higher quality optical cavities will improve the purity of the device and improve the collection efficiency. We also expect greater indistinguishability from resonance fluorescence with the exciting light guided through the diode cavity.³¹ Together, these improvements will allow this scalable platform to be deployed in a wide range of new applications such as a quantum photonic C-NOT gate.

In conclusion, we have demonstrated a compact device that integrates a reconfigurable loss-loss photonic circuit with an array of independently controlled single quantum dot light sources. We are able to show that photons from separate quantum dots can be made indistinguishable. This is a key requirement of linear optical quantum computing schemes.

We thank E. Murray and T. Meany for assistance at an early stage of this project, R. M. Stevenson for assistance with the superconducting detectors, and Kevin and Trevor for hardware support. We acknowledge funding from the EPSRC for the MBE system used for the growth of the LED. C.D. acknowledges support from the Marie Curie Actions within the Seventh Framework Programme for Research of the European Commission, under Network PICQUE (Grant No. 608062). P.S. acknowledges support from the EPSRC Quantum Communications Hub (Grant No. EP/M013472/1). Data Access: The experimental data used to produce the figures in this paper is publicly available at <https://doi.org/10.17863/CAM.23193>.

¹G. Lifante, *Integrated Photonics* (Wiley, 2003).

²A. Politi, M. G. Cryan, J. G. Rarity, S. Yu, and J. L. O'Brien, *Science* **320**(5876), 646–649 (2007).

³J. Carolan, C. Harrold, C. Sparrow, E. Martín-López, N. J. Russell, J. W. Silverstone, P. J. Shadbolt, N. Matsuda, M. Oguma, M. Itoh, G. D. Marshall, M. G. Thompson, J. C. F. Matthews, T. Hashimoto, J. L. O'Brien, and A. Laing, *Science* **349**(6249), 711–716 (2015).

⁴A. Crespi, R. Ramponi, R. Osellame, L. Sansoni, I. Bogioanni, F. Sciarrino, G. Vallone, and P. Mataloni, *Nat. Commun.* **2**, 566 (2011).

⁵J. C. F. Matthews, A. Politi, A. Stefanov, and J. L. O'Brien, *Nat. Photonics* **3**, 346–350 (2009).

- ⁶L. Sansoni, F. Sciarrino, G. Vallone, P. Mataloni, A. Crespi, R. Ramponi, and R. Osellame, *Phys. Rev. Lett.* **108**(1), 010502 (2012).
- ⁷A. Peruzzo, M. Lobino, J. C. F. Matthews, N. Matsuda, A. Politi, K. Poulios, X.-Q. Zhou, Y. Lahini, N. Ismail, K. Wörhodd, Y. Bromberg, Y. Silberberg, M. G. Thompson, and J. L. O'Brien, *Science* **329**(5998), 1500 (2010).
- ⁸J. B. Spring, B. J. Metcalf, P. C. Humphreys, W. S. Kolthammer, X. M. Jin, M. Barbieri, A. Datta, N. Thomas-Peter, N. K. Langford, D. Kundys, J. C. Gates, B. J. Smith, P. G. Smith, and I. A. Walmsley, *Science* **339**(6121), 798–801 (2013).
- ⁹M. A. Broome, A. Fedrizzi, S. Rahimi-Keshari, J. Dove, S. Aaronson, T. C. Ralph, and A. G. White, *Science* **339**(6121), 794–798 (2013).
- ¹⁰A. Crespi, R. Osellame, R. Ramponi, D. J. Brod, E. F. Galvao, N. Spagnolo, C. Vitelli, E. Maiorino, P. Mataloni, and F. Sciarrino, *Nat. Photonics* **7**, 545–549 (2013).
- ¹¹H. Wang, Y. He, Y.-H. Li, Z.-E. Su, B. Li, H.-L. Huang, X. Ding, M.-C. Chen, C. Liu, J. Qin, J.-P. Li, Y.-M. He, C. Schneider, M. Kamp, C.-Z. Peng, S. Höfling, C.-Y. Lu, and J.-W. Pan, *Nat. Photonics* **11**, 361–365 (2017).
- ¹²B. J. Metcalfe, J. B. Spring, P. C. Humphreys, N. Thomas-Peter, M. Barbieri, W. S. Kolthammer, X.-M. Jin, N. K. Langford, D. Kundys, J. C. Gates, B. J. Smith, P. G. R. Smith, and I. A. Walmsley, *Nat. Photonics* **8**, 770–774 (2014).
- ¹³L.-T. Feng, M. Zhang, Z.-Y. Zhou, M. Li, X. Xiong, L. Yu, B.-S. Shi, G.-P. Guo, D.-X. Dai, X.-F. Ren, and G.-C. Guo, *Nat. Commun.* **7**, 11985 (2016).
- ¹⁴A. Mohanty, M. Zhang, A. Dutt, S. Ramelow, P. Nussenzveig, and M. Lipson, *Nat. Commun.* **8**, 14010 (2017).
- ¹⁵J. W. Silverstone, D. Bonneau, K. Ohira, N. Suzuki, H. Yoshida, N. Lizuka, M. Ezaki, C. M. Natarajan, M. G. Tanner, R. H. Hadfield, V. Zwiller, G. D. Marshall, J. G. Rarity, J. L. O'Brien, and M. G. Thompson, *Nat. Photonics* **8**, 104–108 (2014).
- ¹⁶M. Kues, C. Reimer, P. Roztocki, L. R. Cortés, S. Sciara, B. Wetzel, Y. Zhang, A. Cino, S. T. Chu, E. L. Brent, D. J. Moss, L. Caspani, J. Azaña, and R. Morandotti, *Nature* **546**, 622 (2017).
- ¹⁷R. J. Coles, D. M. Price, J. E. Dixon, B. Royall, E. Clarke, P. Kok, M. S. Skolnick, A. M. Fox, and M. N. Makhonin, *Nat. Commun.* **7**, 11183 (2016).
- ¹⁸K. D. Jöns, U. Rengstl, M. Oster, F. Hagart, M. Heldmaier, S. Bounouar, S. M. Ulrich, M. Jetter, and P. Michler, *J. Phys. D: Appl. Phys.* **48**, 085101 (2015).
- ¹⁹N. Prtljaga, R. J. Coles, J. O'Hara, B. Royall, E. Clarke, A. M. Fox, and M. S. Skolnick, *Appl. Phys. Lett.* **104**(23), 231107 (2014).
- ²⁰G. Kiršanskė, H. Thyrrstrup, R. S. Daveau, C. L. Dreeßen, T. Pregnolato, L. Midolo, P. Tighineanu, A. Javadi, S. Stobbe, R. Schott, A. Ludwig, A. D. Wieck, S. I. Park, J. D. Song, A. V. Kuhlmann, I. Söllner, M. C. Löbl, R. J. Warburton, and P. Lodahl, *Phys. Rev. B* **96**, 156306 (2017).
- ²¹I. E. Zadeh, A. W. Elshaari, K. D. Jöns, A. Fognini, D. Dalacu, P. J. Poole, M. E. Reimer, and V. Zwiller, *Nano Lett.* **16**, 2289–2294 (2016).
- ²²M. Davanco, J. Liu, L. Sapienza, C.-Z. Zhang, J. Vinícius De Miranda Cardoso, V. Verma, R. Mirin, S.-W. Nam, L. Liu, and K. Srinivasan, *Nat. Commun.* **8**, 889 (2017).
- ²³J.-H. Kim, S. Aghaeimeibodi, C. J. K. Richardson, R. P. Leavitt, D. Englund, and E. Waks, *Nano Lett.* **17**(12), 7394 (2017).
- ²⁴R. B. Patel, A. J. Bennett, I. Farrer, C. A. Nicoll, D. A. Ritchie, and A. Shields, *J. Nat. Photonics* **4**(9), 632–635 (2010).
- ²⁵E. B. Flagg, A. Müller, S. V. Polyakov, A. Ling, A. Migdall, and G. S. Solomon, *Phys. Rev. Lett.* **104**, 137401 (2010).
- ²⁶E. Murray, D. J. P. Ellis, T. Meany, F. F. Floether, J. P. Lee, J. P. Griffiths, G. A. C. Jones, I. Farrer, D. A. Ritchie, A. J. Bennett, and A. Shields, *J. Appl. Phys. Lett.* **107**, 171108 (2015).
- ²⁷J. Skiba-Szymanska, A. Jamil, I. Farrer, M. B. Ward, C. A. Nicoll, D. J. P. Ellis, J. P. Griffiths, D. Anderson, G. A. C. Jones, D. A. Ritchie, and A. Shields, *J. Nanotechnol.* **22**, 065302 (2011).
- ²⁸K. D. Jöns, P. Atkinson, M. Müller, M. Heldmaier, S. M. Ulrich, O. G. Schmidt, and P. Michler, *Nano Lett.* **13**(1), 126–130 (2013).
- ²⁹A. J. Bennett, R. B. Patel, J. Skiba-Szymanska, C. A. Nicoll, I. Farrer, D. A. Ritchie, and A. Shields, *J. Appl. Phys. Lett.* **97**, 031104 (2010).
- ³⁰J. P. Lee, E. Murray, A. J. Bennett, D. J. P. Ellis, C. Dangel, I. Farrer, P. Spencer, D. A. Ritchie, and A. Shields, *J. Appl. Phys. Lett.* **110**(7), 071102 (2017).
- ³¹A. Müller, E. B. Flagg, P. Bianucci, X. Y. Wang, D. G. Deppe, W. Ma, J. Zhang, G. J. Salamo, M. Xiao, and C. K. Shih, *Phys. Rev. Lett.* **99**(18), 187402 (2007).